Supporting Information

Programmable, UV Printable Dielectric Elastomers Actuate at Low Voltage without Prestretch and Supporting Frames

Ramadan Borayek[a], Pengpeng Zhang[b], Habimana J. Willy[a], Mostafa Zedan[c], Jian Zhu[b] and Jun Ding[a]*

[a] Department of Materials Science and Engineering, Faculty of Engineering, National University of Singapore, 9 Engineering Drive 1, Singapore 117575.

[b] Department of Mechanical Engineering, Faculty of Engineering, National University of Singapore, 9 Engineering Drive 1, 117575, Singapore.

[c] Institute of Materials Research and Engineering, Agency for Science, Technology and Research (A*STAR), 138634, Singapore.

[*]Corresponding author (msedingj@nus.edu.sg)

S1. Elastomers printing

Resin Working Curve. The resin working mechanism (cured depth at various UV light exposure time) was estimated by using Asiga Pico2™ HD 385 nm (Asiga; Australia), liquid based DLP printer. The UV light source power measured by the internal radiometer was 15.68 mW.cm^{-2}. The cured depth relationship with the exposure energy can be described by the following equation:

$$\boldsymbol{C_d = D_P \ln\left(\frac{E}{E_c}\right)} \quad \textbf{(1)}$$

Where C_d is the cured depth, D_P is the resin penetration depth, E is the exposure energy, and E_C is the critical exposure energy to initiate the photopolymerisation process. From the plot of the resin working mechanism **Figure S1a,** the thickness of the cured depth can be calculated and controlled by the variation of the light absorber amount. Also the cured thickness has been controlled by the variation of the photoinitiator amount as shown in **Figure S1b**.

Table S1. Printing parameters values for successfully printed parts from different elastomers formulations of 100µm layer thickness using Asiga printer.

Formulation	layer thickness	bottom exposure time	burn in layers	exposure time	separation velocity	separation distance	approach velocity
D0	100µm	7 sec	1	4 sec	2mm/sec	25mm	3.5mm/sec
D05	100µm	6.2 sec	1	3.75 sec	2mm/sec	25mm	3.5mm/sec
D10	100µm	5.8 sec	1	3.5 sec	2mm/sec	25mm	3.5mm/sec
D15	100µm	5 sec	1	3.2 sec	2mm/sec	25mm	3.5mm/sec
D20	100µm	4.75 sec	1	2.9 sec	2mm/sec	25mm	3.5mm/sec

Table S2: chemical formulations compositions and summary of mechanical results for elastomers resulted from the printings of the different formulations

Name	Monomer (HPA) Vol%	Cross-linker	Photo-initiator (TPO)	Light absorber (gr/100ml)	Ultimate tensile strength	Max. strain (%)

		(DEG) Vol%	wt%		(MPa)	
D0	100	0	1	0.05	1.39	610
D05	95	5	1	0.05	1.22	690
D10	90	10	1	0.05	1.15	740
D15	85	15	1	0.05	0.95	800
D20	80	20	1	0.05	0.81	860

S2. FTIR and UV light absorbance characterization

FTIR Analysis. The FTIR analysis has been performed for the liquid monomer and solid polymer films of 1mm thickness at room temperature using FTIR spectroscopy (Spectrum 2000, Perkin Elmer) under attenuated total reflection mode. In the ATR spectrum of monomers (**Figure S3c**), the polar carbonyl group (C=O stretching) has a peak at 1715 cm^{-1}, while after polymerization, it is slightly shifted to 1717 cm^{-1}. The peak of the hydroxyl group (OH) can be observed at 1298 cm^{-1}. The carbon double bond peaks are observed at 1620 and 940 cm^{1}, while it disappeared after polymerization as evidence of the conversion of the monomers to a stretchable polymer. The ester peak (C-O stretching) has a peak at 1200 cm^{-1}. The stability of this formulation in a normal environment not absorbing moisture comes from the use of the methyl group (CH_3) which is attached to the propyl group. The existence of the methyl groups can reduce the available locations for hydrogen bonding reaction to give the polymer film good stability in the normal environment, which solving a serious problem for the acrylate-based dielectric elastomer.

UV Transmittance Analysis. The transmittance was measured using UV spectrometer (UV-1800, Shimadzu) for a 1mm thickness sample and results showed that the sample has a transmittance of 85% at 500nm (**Figure S3d**).

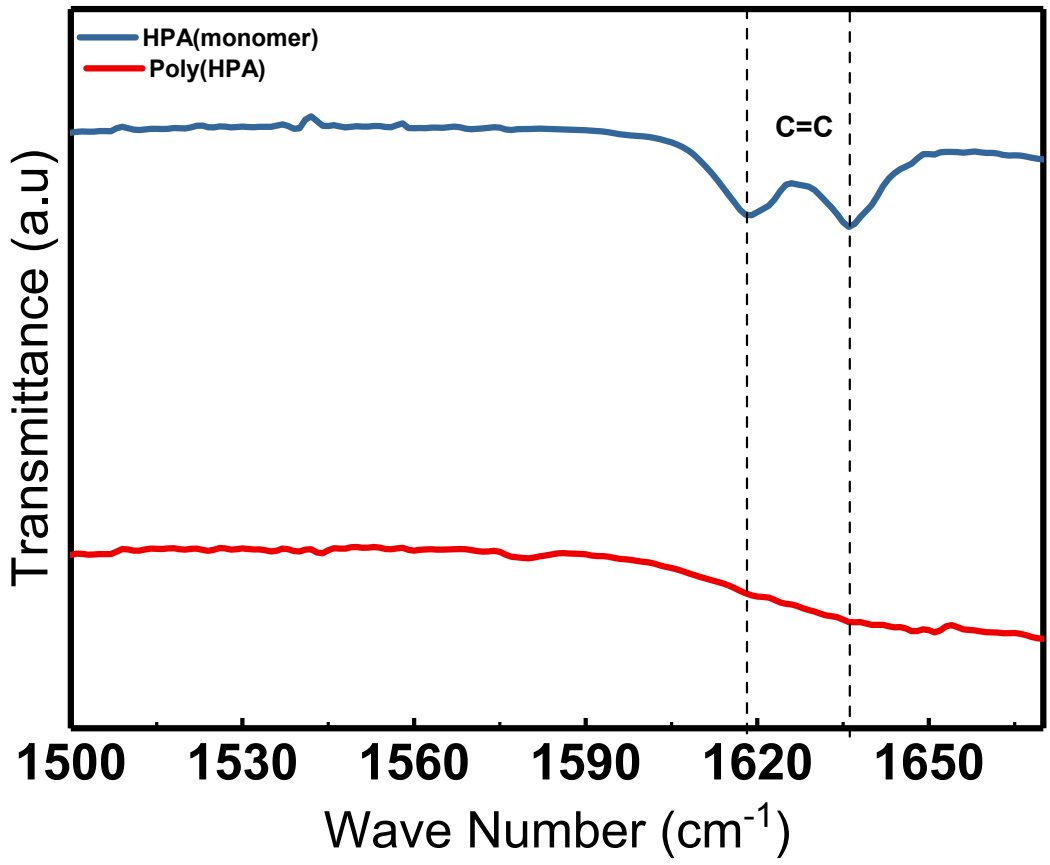

Figure S1. FTIR results for liquid HPA monomer and P(HPA) at the c=c band spectrum.

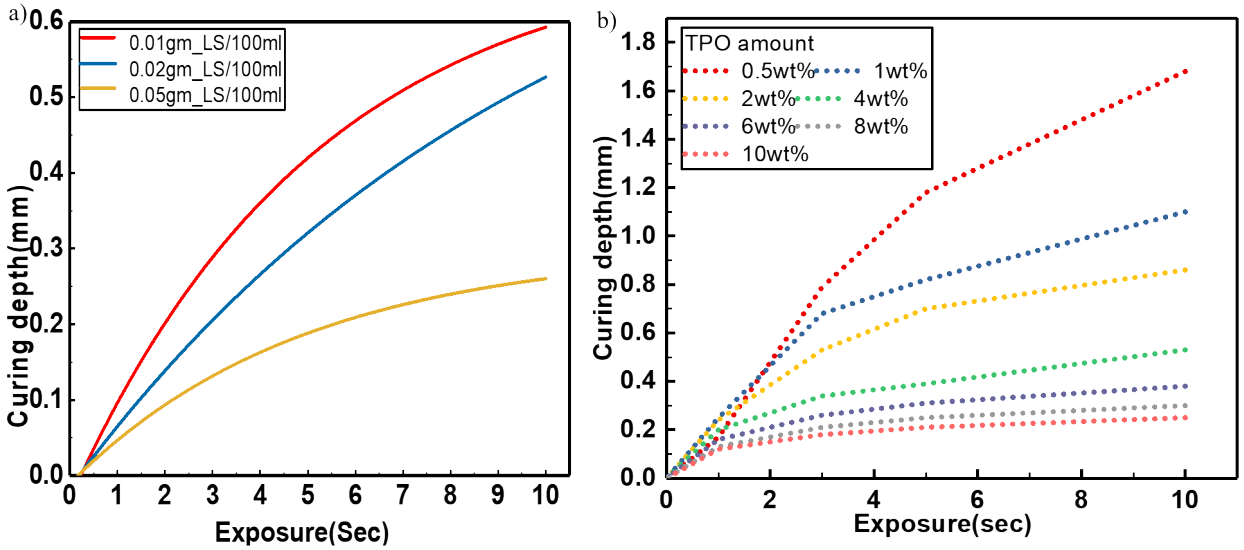

Figure S2. **a)** Curing depth versus exposure time for different light stabilizers amounts. **b)** Curing depth versus exposure time for different amounts of photoinitiator.

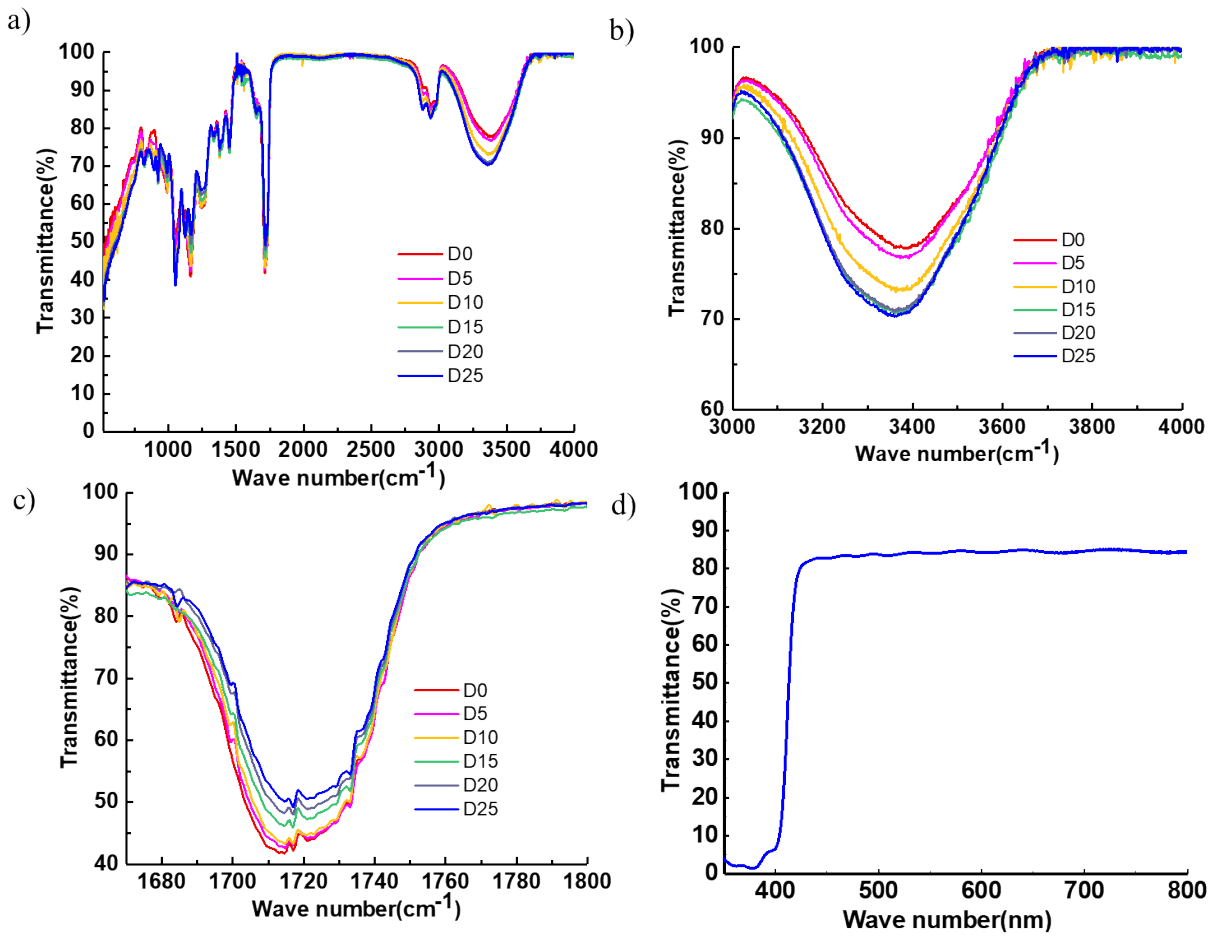

Figure S3. a) FTIR full spectrum results for the investigated elastomers, b) FTIR spectrum results showing OH stretching peaks for different mixing ratios of HPA with DEG, c) FTIR spectrum results showing C=O stretching peaks for different mixing ratios of HPA with DEG, d) Transmittance of the printed elastomer from D20 showing high transparency.

S3. Thermal and gel extraction characterization results

Figure S4a showing the full spectra of the Thermogravemetric results for the different elastomers resulted from the printing of all the formulations. It's obvious that with increasing the DEG content in the elastomer formulations, the losing weight against temperature is increasing. The reason behind the weight loos is due to the evaporation of the plasticizer, DEG, or may be due to the evaporation of the pendant water molecules due to the formation of H bonding with the hydroxyl groups. From **Figure S4b**, we can realize that the glass transition temperature decreases with the increase of the plasticizers content in the formulations until it reaches -53^{o}C for D25.

The gel extraction efficiency results are depicted in **Figure S4c**. With increasing the content of the plasticizer, DEG, the extraction efficiency is highly drops to reach 67% for D25.

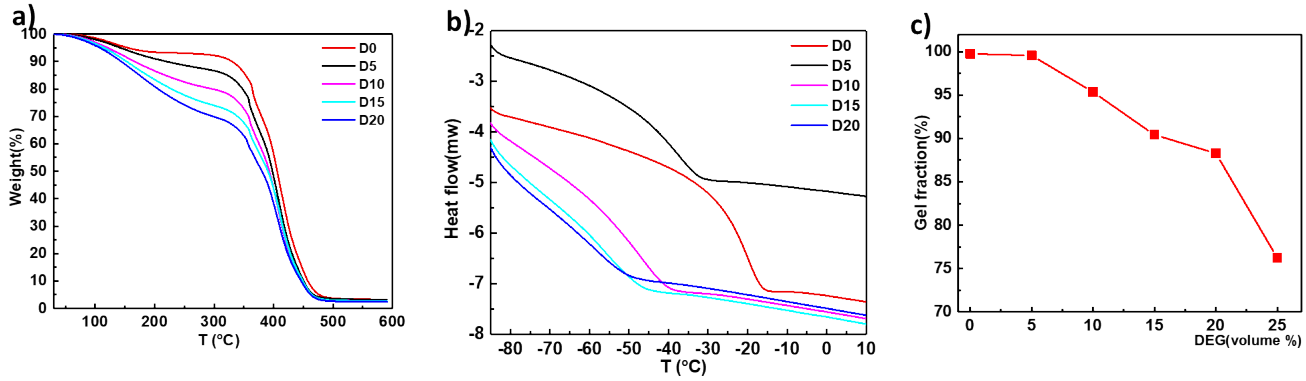

Figure S4. a) TGA results for the investigated elastomers, b) DSC results for the different elastomers and c) Gel extraction efficiency results for elastomers resulted from different mixing ratios of HPA with DEG.

S4. Mechanical, Electrochemical and electromechanical characterization results

Figure S5a showing the variation of the conductivity with frequency in the range of 1Hz to 1MHz. The results confirm that the conductivity of the elastomers are very low and in the range of the dielectric elastomers values. Also, it's obvious that by increasing the content of the plasticizers amount in the formulations, the conductivity increased to reach 10^{-7} S/cm for D25. The increase in the conductivity has witnessed an increase in the losses as shown in Figure S5b for the imaginary part of the dielectric constant and Figure S5c for tan(δ).

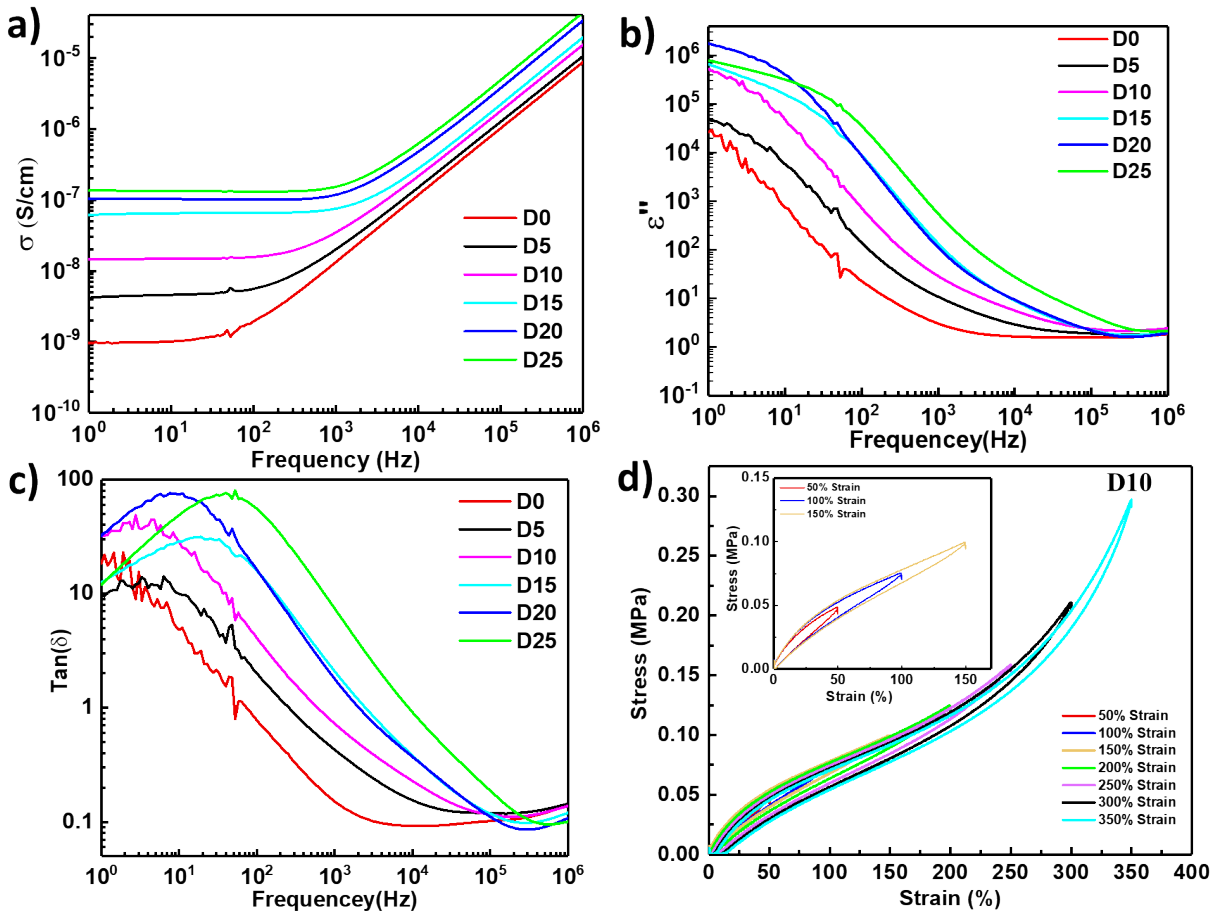

Figure S5. Electrochemical results of the investigated elastomers showing the variation of a) conductivity, b) imaginary dielectric constant and c) tan($^{\delta}$) with the frequency, d) Cyclic stress strain of elastomer fabricated from material D0 (All other elastomers material have same elastic behavior).

Figure S6 is describing the behavior of the elastomers under the electric field. As depicted in Figure S6a, by applying an electric field on the sides of the elastomers, the elastomers bent to the side of the positive electrode. The bending increases by increasing the electric field value to reach the maximum bending angle (45^{o}) at an applied voltage of 3Kv, but results cannot repeated. By increasing the value of the voltage, no increase in the bending angle has been observed, as illustrated in Figure S6a. Figure S6b is showing the response of the elastomers under the electric field after charging the elastomers but this time by opposing the polarity. We noticed that the

elastomers bend immediately to the side of the positive electrode but by increasing the time, the elastomers start to return to the initial state. The average time for the elastomers to return to the initial state was found to be around 400 sec.

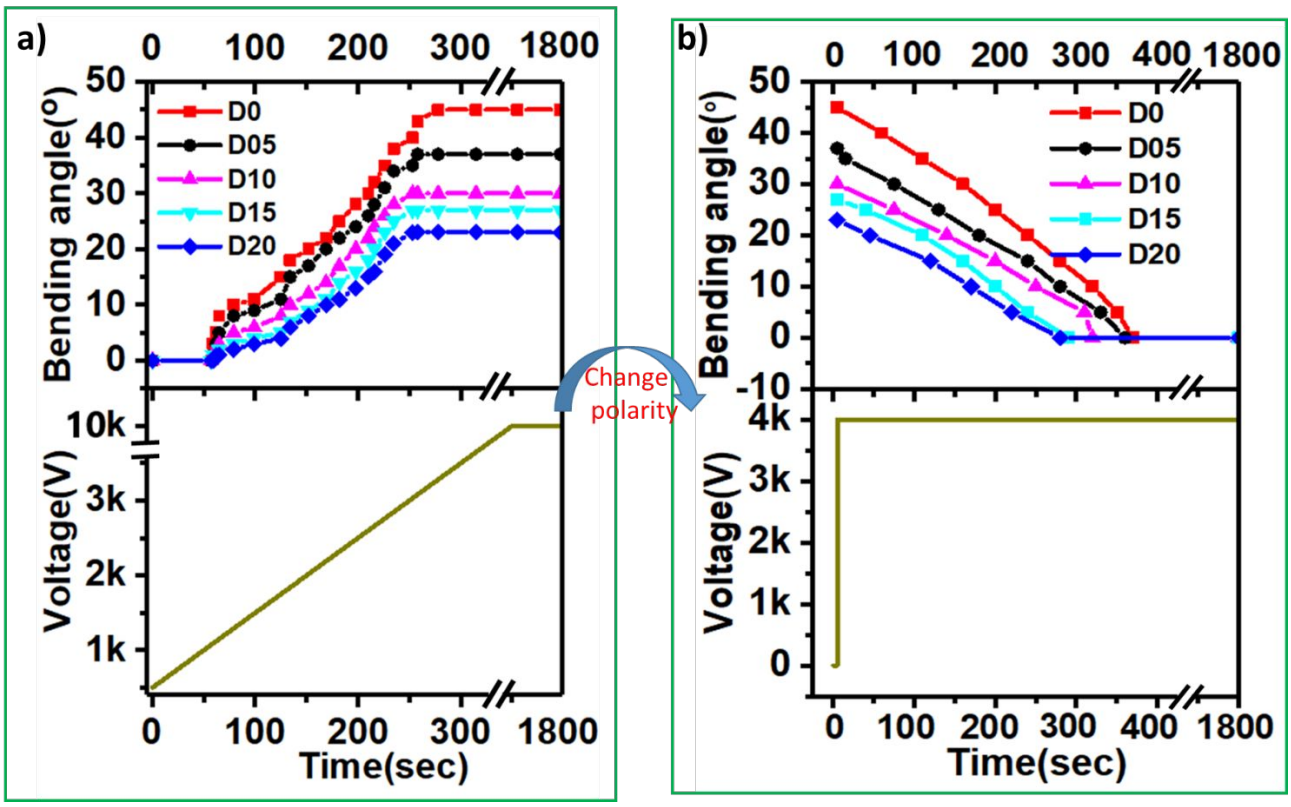

Figure S6. a) Response of the investigated elastomers during the charging cycle (elastomers here bent to the side of the positive electrode), b) Response of the investigated elastomers under constant voltage after changing the polarity and after the charging cycle.

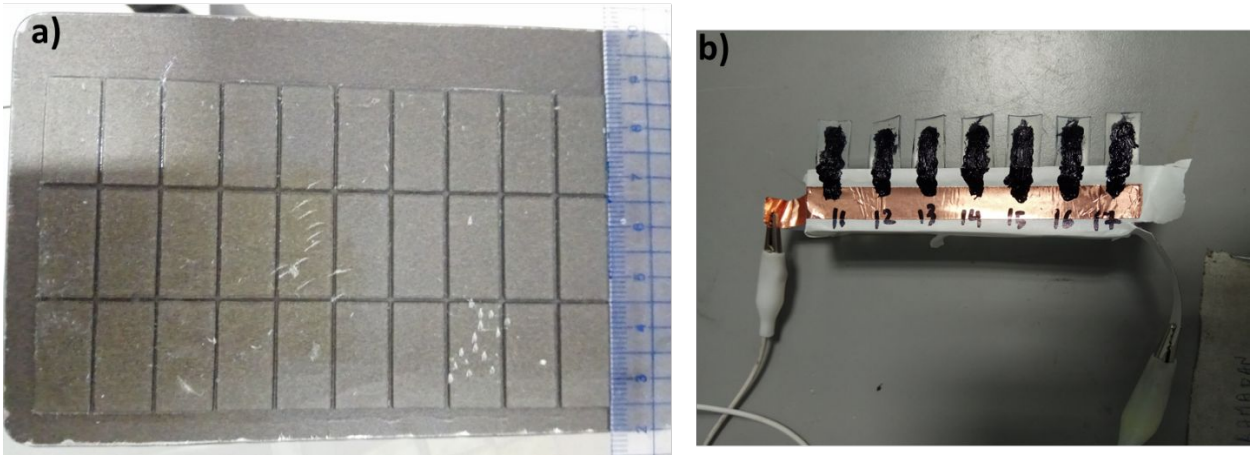

Figure S7. a) Set of 30 samples printed one patch for testing the bending direction , b) simple test rig to randomly test the printed samples from different patches (sample number 16 denotes to patch 1 with sample number 6).

S5. Simulation of nonlinear electromechanical coupling in the dielectric elastomer

Mechanical behavior of elastomer material was modeled using nonlinear model approximated from experimental measurement. Yeoh's model has shown the best fit as presented in **Figure S7**. For small deformation less than 20%, the material behavior can be approximated by a linear model with the experimental values of linear Young's Modulus for each material type. A Poisson's ration of 0.49 as a typical for elastomers was used.

The geometry of the model is built in the concept of a dielectric material (elastomer) with a thickness Z, confined between two conducting surfaces of negligible thickness (carbon grease), **Figure S8a**. The whole set is surrounded by air; the dielectric constant of air being 1. For the elastomer, the measured value of dielectric constant was used. The distribution of Maxwell's stresses in the actuated area is depicted in **Figure S8b**.

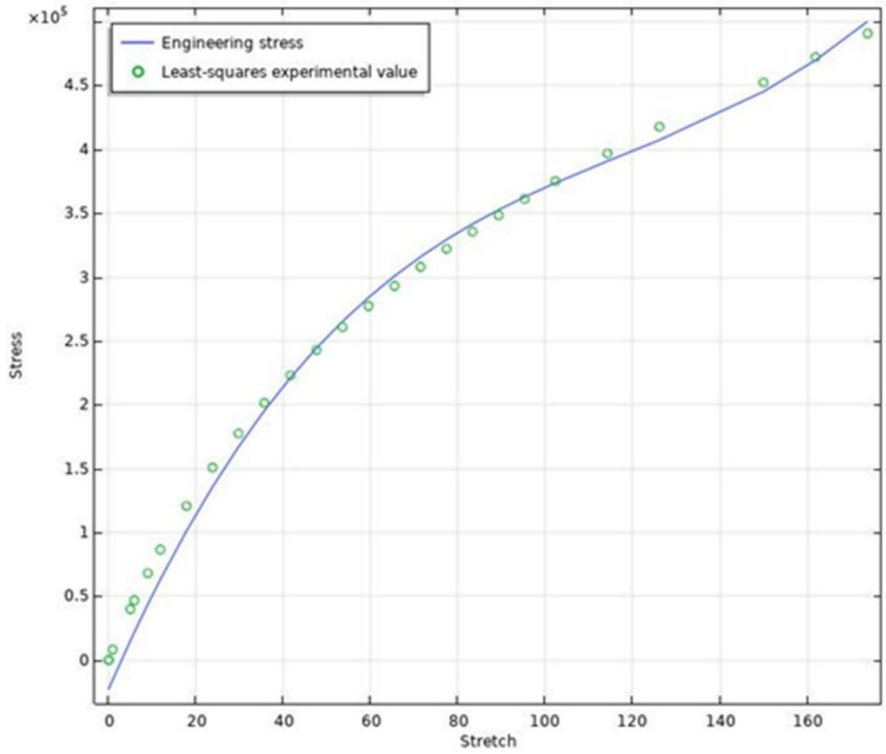

Figure S8. Yeoh's model fitting of experimental data of our material, results of D0 has been presented here.

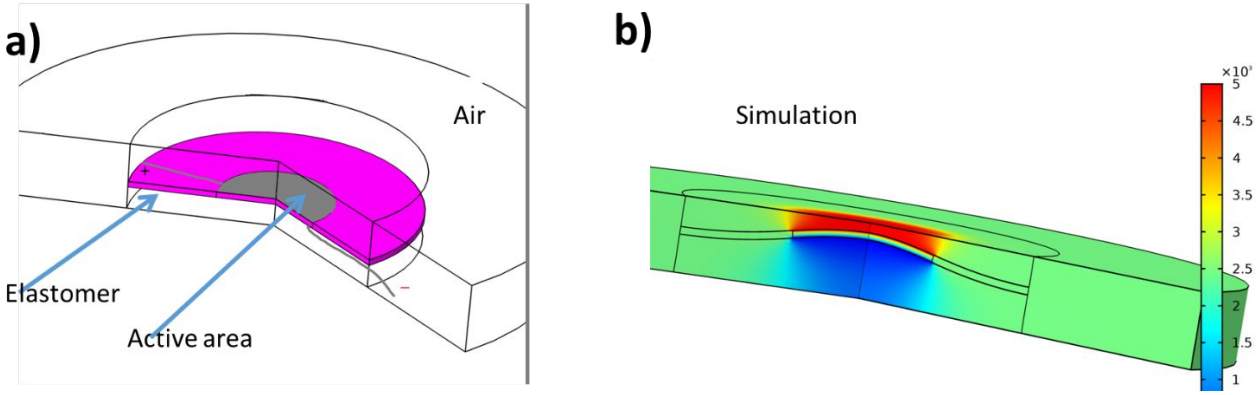

Figure S9. a) The model and assumptions proposed for modelling electromechanical behavior of the elastomers, b) The distribution of Maxwell's stresses in the actuated area.

The dependence of the bending displacement on the applied voltage is shown in **Figure S9.** As shown in Figure S9, it is obvious that the elastomer of D0 material characteristics can start to provide obvious bending deformation at an applied voltage of 1640V for a sample with 1mm thickness, 10mm width and 40mm length.

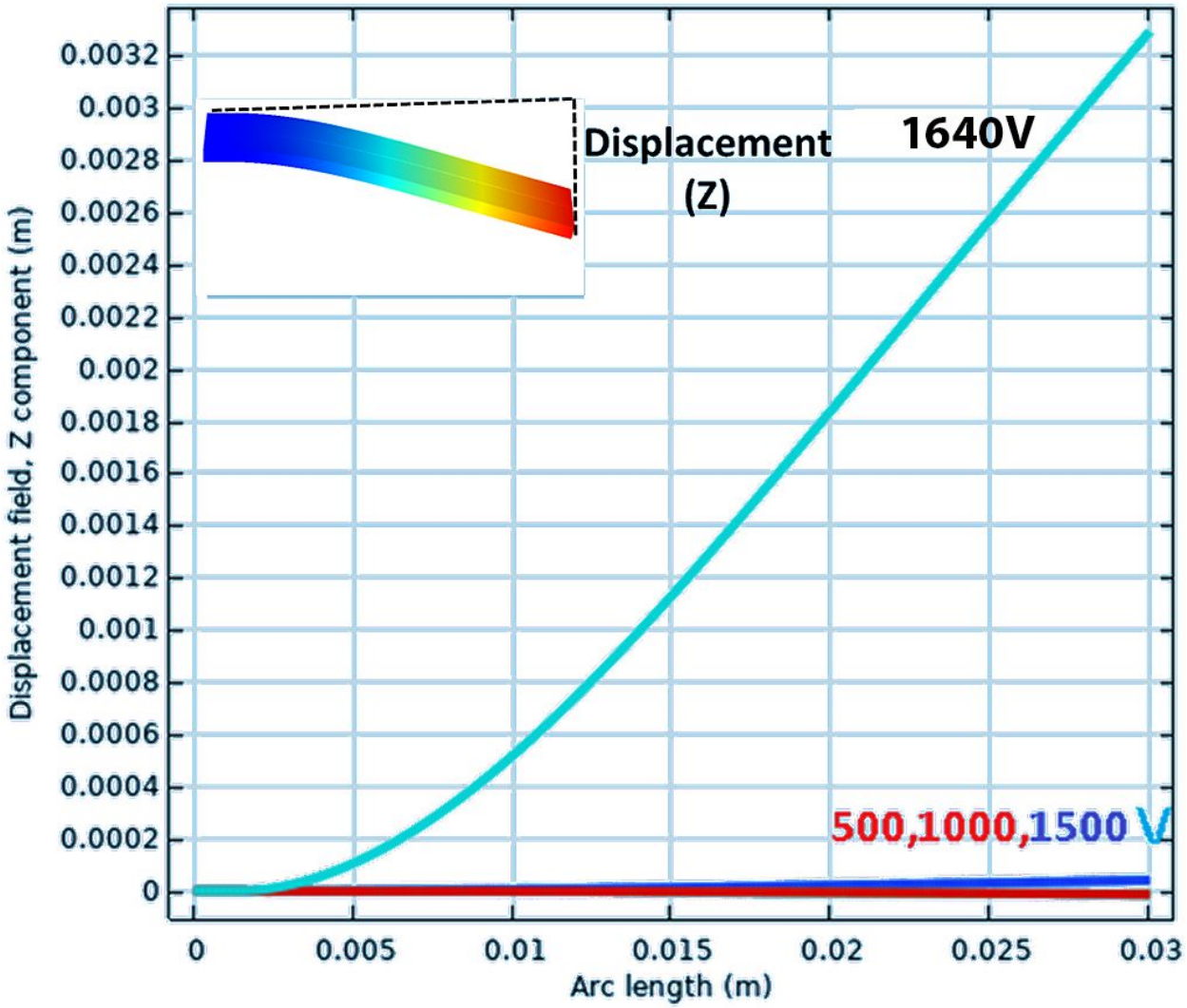

Figure S10. a) simulations results showing the dependence of Z bending displacement on the applied voltage for a unimorph sample without pre-stretching and without adding passive layers, sample dimension is 10mm in width,40mm in length, 1mm in thickness, materials properties used is D0.

Electromechanical coupling was approximated by a combination of both Maxwell contributions from the parallel charged surfaces, and electrostriction contribution. In vacuum (no magnetic field), the electromagnetic stress tensor is shown in **Equation 2**:

$$\boldsymbol{\sigma_{EM\_vacum} = \varepsilon_o E_i E_j - \frac{1}{2}(\varepsilon_o E^2) I} \quad \textbf{(2)}$$

Where $\boldsymbol{\varepsilon_o}$ is the permittivity of free space, **E** is the electric field and **I** is the identity matrix. In case of a dielectric material under assumption of an isotropic linear material, the finite

deformation theory defines the small strain tensor (Green-Lagrangian strain tensor) as in **Equation 3** below.

$$\boldsymbol{T} = \frac{\mathbf{1}}{\mathbf{2}}[(\nabla \boldsymbol{u})^{\boldsymbol{T}} + \nabla \boldsymbol{u} + (\nabla \boldsymbol{u})^{\boldsymbol{T}}(\nabla \boldsymbol{u})] \quad \textbf{(3)}$$

In **Equation 3**, $\boldsymbol{u}$ is the deformation vector. The electric susceptibility when the material is under electromagnetic stress can be given as in **Equation 4** as a function of $\boldsymbol{T}$;

$$\boldsymbol{\chi} = \boldsymbol{\chi_o} + \left(\frac{\boldsymbol{a_1 - a_2}}{\boldsymbol{\varepsilon_o}} - \mathbf{2}\boldsymbol{\chi_o}\right)\boldsymbol{T} + \left(\frac{\boldsymbol{a_2}}{\boldsymbol{\varepsilon_o}} + \boldsymbol{\chi_o}\right)\boldsymbol{tr}(\boldsymbol{T})\boldsymbol{I} \quad \textbf{(4)}$$

where $\boldsymbol{\chi_o}$ is the electric susceptibility before deformation, $\boldsymbol{tr}(\boldsymbol{T})$ is the trace of the small strain tensor and $\boldsymbol{a_1}, \boldsymbol{a_2}$ are coefficients characterizing the electrostriction response of the material when subjected to deformation in external electric field. From the expression of the electric susceptibility, the electromagnetic strain tensor becomes:

$$\boldsymbol{\sigma_{EM}} = \boldsymbol{\varepsilon_o \varepsilon_r E_i E_j} - \frac{\mathbf{1}}{\mathbf{2}}\left(\boldsymbol{\varepsilon_o \varepsilon_r E^2}\right)\boldsymbol{I} + \frac{\mathbf{1}}{\mathbf{2}}[(\boldsymbol{a_2 - a_1})\boldsymbol{E_i E_j} + \boldsymbol{a_2 E^2 I}] \quad \textbf{(5)}$$

However, in literature,[1–3] available experimental data of the electrostriction coefficients are defined in a different formalism; originating from the series approximation of the polarization in case of a non-linear material response to the applied field. In this formalism, the nonlinear electromechanical interaction can be expressed through **Equation 5**; where the linear term is associated with the piezoelectric effect and coefficients $\boldsymbol{g_{ijm}}$, are piezoelectric coefficients. The quadratic effect is associated with the electrostriction with coefficients$\boldsymbol{Q_{ijmn}}$, which form a 4th order tensor, called electrostriction coefficients.

$$\boldsymbol{u_{ij}} = \boldsymbol{g_{ijm} P_m} + \boldsymbol{Q_{ijmn} P_m P_n} + \ldots \quad \textbf{(6)}$$

The polarization-related 4th order tensor $\boldsymbol{Q_{ijmn}}$can be written in a collapse Voigt form as $\boldsymbol{Q_{ij}}$. In the electrostriction matrix for isotropic polymers in a one-dimensional oriented electric only $\boldsymbol{Q_{11}}$ and Q_{12} are needed [4]. It is common to measure the hydrostatic electrostriction coefficient $\boldsymbol{Q_h} = (\boldsymbol{Q_{11} - 2Q_{12}})$. From fitting of existing experimental data, it was demonstrated that there is

a linear dependence between the $\boldsymbol{Log(Q_h)}$ and $\boldsymbol{Log(S/\varepsilon_0\varepsilon_r)}$ [4]. We used this relationship to estimate $\boldsymbol{Q_h}$and then $\boldsymbol{Q_{11}}$ and $\boldsymbol{Q_{12}}$ for our material based on measured $\boldsymbol{\varepsilon_r}$ and stiffness. In turn, the electrostriction coefficients in the electromagnetic stress tensor are deduced using the formula in the system of **Equation 7** and used in COMSOL software which uses the right-Cauchy deformation tensor to account for total deformation in solids.[4]

$$\begin{cases} a_1 = -2\,\varepsilon_0^2\,\chi_0^2\,Y_M \frac{Q_{11}(1-\upsilon)+2\upsilon Q_{12}}{(1+\upsilon)(1-2\upsilon)} \\ a_1 = -2\,\varepsilon_0^2\,\chi_0^2\,Y_M \frac{Q_{11}(1-\upsilon)+Q_{12}}{(1+\upsilon)(1-2\upsilon)} \end{cases} \quad \textbf{(7)}$$

In the expression, $\boldsymbol{Y_M}$ is the estimated Young's modulus and $\boldsymbol{\upsilon}$ the Poisson's ratio.

Reference

(1) Pelrine, R.; Kornbluh, R.; Joseph, J.; Heydt, R.; Pei, Q.; Chiba, S. High-Field Deformation of Elastomeric Dielectrics for Actuators. *Mater. Sci. Eng. C* **2000**, *11*, 89–100.

(2) Newnham, R. E.; Sundar, V.; Yimnirun, R.; Su, J.; Zhang, Q. M. Electrostriction: Nonlinear Electromechanical Coupling in Solid Dielectrics. *J. Phys. Chem. B* **1997**, *101*, 10141–10150.

(3) Li, F.; Jin, L.; Xu, Z.; Zhang, S. Electrostrictive Effect in Ferroelectrics: An Alternative Approach to Improve Piezoelectricity. *Appl. Phys. Rev.* **2014**, *1*, 011103.

(4) COMSOL Inc. COMSOL Multiphysics® Modeling Software. COMSOL Inc 2017.